A redox-flow battery with an alloxazine-based organic electrolyte

A redox flow battery with an alloxazine-based organic electrolyte

Kaixiang Lin[1], Rafael Gómez-Bombarelli[1], Eugene S. Beh[1,2], Liuchuan Tong[1], Qing Chen[2], Alvaro Valle[3], Alán Aspuru-Guzik[1], Roy G. Gordon[1,2*], Michael J. Aziz[2*]

[1] *Department of Chemistry and Chemical Biology, Harvard University, 12 Oxford Street, Cambridge, Massachusetts 02138, USA*

[2] *Harvard John A. Paulson School of Engineering and Applied Sciences, 29 Oxford Street, Cambridge, Massachusetts 02138, USA*

[3] *Harvard College, Cambridge, Massachusetts 02138, USA*

*E-mail: RGG (gordon@chemistry.harvard.edu) and MJA (aziz@seas.harvard.edu)

Redox flow batteries (RFBs) can store large amounts of electrical energy from variable sources, such as solar and wind. Recently, redox-active organic molecules in aqueous RFBs have drawn substantial attention due to their rapid kinetics and low membrane crossover rates. Drawing inspiration from nature, here we report a high-performance aqueous RFB utilizing an organic redox compound, alloxazine, which is a tautomer of vitamin B_2's isoalloxazine backbone. It can be synthesized in high yield at room temperature by single-step coupling of inexpensive *o*-phenylenediamine derivatives and alloxan. The highly alkaline-soluble alloxazine 7/8-carboxylic acid (ACA) produces a RFB exhibiting open-circuit voltage approaching 1.2 volts and current efficiency and capacity retention exceeding 99.7% and 99.98% per cycle, respectively. Theoretical studies indicate that structural modification of alloxazine with electron donating groups should allow further

increases in battery voltage. As an aza-aromatic molecule that undergoes reversible redox cycling in aqueous electrolyte, alloxazine represents a ~~new~~ class of radical-free redox-active organics for use in large-scale energy storage.

Improved methods for storing electrical energy from intermittent renewable sources are needed to support the rapid deployment of photovoltaic (PV) and wind power.[1–3] A promising approach for safe and cost-effective stationary energy storage uses redox flow batteries (RFBs), in which the energy is stored in fluids held outside the power conversion electrochemical cell.[4,5] This permits the independent engineering of energy (electrolyte volume and/or concentration) and power (cell area) capacities and enables the attainment of the high energy-to-power ratios (i.e. long discharge durations at rated power) necessary to deliver energy from PV and wind when it is needed. Since the invention of RFBs in the 1970s, the development efforts for its electrolyte materials – the core component of RFBs – have concentrated on single metal ions such as vanadium, iron and chromium, where the battery voltages are fixed by the reduction potentials of these ions, and their solubilities and stabilities are governed by the pH and composition of the supporting electrolyte.[6,7] However, their development has been impeded by one or more shortcomings such as high electrolyte corrosivity, toxicity, cost, membrane cross-over rate, or sluggish reaction kinetics.

Contrary to the limited numbers of metal ions suitable for RFBs, organic molecules display high chemical diversity, allowing optimization of electrolyte properties such as higher solubility (by adding solubilizing groups), higher voltage (by varying the electron donating properties of functional groups), and lower membrane cross-over rate (by tuning the molecular size or net charge on the molecules). Recently, researchers have

demonstrated RFBs of much improved performance by rational design of organic-based electrolyte materials (summarized in Table 1).[8–13] For instance, Huskinson *et al.* utilized a sulfonic-acid functionalized 9,10-anthraquinone, which showed fast kinetics and high solubility in a supporting electrolyte of sulfuric acid; by pairing it up with cheap bromine/hydrobromic acid, the team showed approximately a three-fold reduction of the potential cost of electrolyte materials, compared with state-of-art all-vanadium RFBs.[8,9] The toxicity and corrosivity of bromine, however, limit its use to industrial and utility settings. By switching from acidic to alkaline supporting electrolyte, Lin *et al.* demonstrated a less corrosive and non-toxic RFB using hydroxylated 9,10-anthraquinone and a food additive, ferrocyanide, targeted for residential and commercial usage.[10] To reduce membrane cost while maintaining a low membrane crossover rate, Janoschka *et al.* prepared polymeric methyl viologen and (2,2,6,6-tetramethylpiperidin-1-yl)oxidanyl (TEMPO) which showed almost no sign of membrane crossover when cheap dialysis membranes were used in place of expensive cation-exchange membranes.[11] Despite these great advances, each system still has potential for further improvement, such as replacing toxic halogen species with high-performance organic molecules, increasing the ion conductivity and energy density of alkaline systems, and reducing the high electrolyte viscosity associated with the dissolution of polymers at practical concentrations. To accelerate the development of organic-based RFBs, more compounds with useful redox potential, high solubility, and ease of synthesis are highly desired. Previous aqueous organic-based RFBs have utilized only three types of stable redox-active species: **1)** quinones, **2)** TEMPO and **3)** methyl viologen, as shown in Table 1. To date, tailored improvements have been proven possible only in quinone systems.

Gaining inspiration from naturally occurring flavin cofactors, here we report a novel alloxazine-based aqueous organic RFB. Alloxazines can be synthesized via a simple and high-yielding coupling reaction between *o*-phenylenediamine derivatives and alloxan in acetic acid and boric acid at room temperature and atmospheric pressure (Table 2).[14–16] Functionalization of alloxazine with a carboxylic acid group renders the alloxazine molecule highly soluble in alkaline solution – up to 2 M in pH 14 KOH, which corresponds to a charge density of 108 Ah/L. By pairing it up with ferri/ferrocyanide as the positive electrolyte, we built a high-performance RFB characterized by an open-circuit voltage approaching 1.2 V and current efficiency and capacity retention exceeding 99.7% and 99.98% per cycle, respectively. Enabled by a high-throughput computational study, a relationship between different alloxazine functional groups and their effects on reduction potential was established and exploited to guide the design of future alloxazine-based electrolyte materials. For instance, by replacing the carboxylic acid group with another alkaline-soluble hydroxyl group, the battery voltage can be further raised by almost 10%.

Rational Design of Electrolyte Material

Designing an appropriate organic molecule as electrolyte material starts from identifying redox-active cores followed by functionalization of the core structure to achieve a practical reduction potential and solubility. We observed that riboflavin 5' phosphate (FMN), a highly water-soluble compound derived from vitamin B_2, undergoes two-electron reduction *via* a flavin semiquinone radical intermediate on its isoalloxazine backbone (Supplementary Fig. 1).[17,18] In alkaline solution, it exhibited high reversibility and a low reduction potential of −0.53 V vs. SHE (Fig. 1a). Further exploration of its

isoalloxazine motif led to the discovery that lumichrome, an alloxazine derivative that differs from isoalloxazine by its diazabutadiene double bond configuration, exhibited a much lower reduction potential of −0.70 V vs. SHE (Fig. 1b). Alloxazine had previously been studied in the solid state as an anode material for non-aqueous lithium and sodium ion batteries.[19] However, the low solubility of alloxazine in a wide range of solvents presents a challenge for solution-phase applications. To increase its solubility in aqueous solution, we functionalized the alloxazine core with an alkali-soluble carboxylic acid group by coupling *o*-phenylenediamine-4-carboxylic acid (a.k.a. 3,4-diaminobenzoic acid) with alloxan to afford an isomeric mixture of alloxazine 7/8-carboxylic acid (ACA) in almost 100% yield (Supplementary Fig. 2). The reduction potential of ACA from CV measurement is −0.62 V vs. SHE (Fig. 1c). The larger separation between its oxidation and reduction peaks than those of FMN and lumichrome is likely due to slower kinetics. From our rotating disk electrode (RDE) measurement, the reduction rate constant was measured to be $1.2\pm0.2 \times 10^{-5}$ cm s^{-1} (Supplementary Fig. 3). Nevertheless, this value is still an order of magnitude higher than that of the slower side of all-vanadium RFBs.[6]

Besides the large shift in reduction potential moving from isoalloxazine to alloxazine, we also observed a significant increase in chemical stability in alkaline conditions. Whereas cyclic voltammetry (CV) measurement of 0.5 M FMN in an alkaline solution revealed an almost 70% decrease in reduction signal within 2 weeks, an ACA solution at the same concentration showed almost no sign of degradation (Supplementary Fig. 4). Quantification of ACA stability was achieved by proton nuclear magnetic resonance (^{1}H NMR) analysis of a 0.5 M solution of ACA maintained at pH 14 over the course of six weeks. The decomposition of ACA, assuming first-order kinetics (R^2 =

0.991), had a rate constant of 1.39×10^{-3} day^{-1}, equivalent to a solution half-life of 500 days (Supplementary Fig. 5). This combination of lower reduction potential (−0.62 V vs. −0.53 V) and higher chemical stability (500 days vs. 10 days half-life of FMN at pH 14), made ACA a much better candidate for an electrolyte material.

Electrochemical Full-cell Study

To demonstrate ACA in a full cell, we paired ACA with ferri/ferrocyanide (Fig. 1c and d). The battery was assembled using 0.5 M ACA (1.5 mmol) as the negative electrolyte and 0.4 M ferrocyanide (4.5 mmol) + 40 mM ferricyanide (0.46 mmol) as the positive electrolyte. Both solutions were adjusted to pH 14 by KOH. Excess quantities of ferrocyanide and ferricyanide were used to ensure the negative terminal remained the capacity-limiting side for the purpose of evaluating its electrochemical stability during cycling. The resulting alkaline aqueous RFB showed an open-circuit voltage (OCV) approaching 1.2 V. The OCV versus state-of-charge (SOC) monotonically increased from 10% to 90% SOC (Fig 2a). Polarization studies conducted at room temperature showed a peak power density of 0.35 W cm^{-2} at a current density of 0.58 A cm^{-2}. The linearity of the polarization curves allows us to derive a polarization area-specific resistance (ASR), which is 1.03 Ω cm^2 at 50% SOC. About 70% of this cell ASR is contributed by the membrane (Supplementary Fig. 6), similar to our previous observation.[10] Note that ACA redox kinetics does not show up as a significant kinetic overvoltage loss (i.e. a non-linearity at the low overvoltage region) in the polarization curve, likely owing to the large surface area provided by the porous carbon electrodes. The electrochemical stability of ACA was evaluated based on an extended charge-discharge study over 400 cycles (Fig. 2c). The current efficiency exceeded 99.7% at 0.1 A cm^{-2}, which is indicative of

negligible side reactions during cell cycling and a low crossover rate through the membrane. The round-trip energy efficiency in this cycling experiment averaged around 63%. The battery exhibited a remarkably high capacity retention rate of more than 91% over 400 cycles, or a capacity loss rate of 0.023% per cycle. To further analyze capacity retention, we compared the total charge from the cell before and after cycling using chronoamperometry to charge and discharge the cell at constant voltage (Supplementary Fig. 7). From this result, the measured capacity retention from 400 cycles was 95%, i.e. the loss rate was 0.013% per cycle. We believe the discrepancy between this measurement and the capacity retention observed during constant-current cycling was due to an increase of system resistance (which we infer from decreasing energy efficiency with cycle number); this effect moved the charging and discharging curves closer to the cutoff voltages, resulting in less complete charging and discharging with increasing cycle count (Supplementary Fig. 8). We expect further cell development, including variations in pH, membrane and sealing method, to lead to further improvement of capacity retention. By increasing the concentration of ACA to 1 M, we increased the electrolyte charge density by almost two-fold (Supplementary Fig. 9a). Together with adjusted cell compression and higher ACA concentration, we were able to improve round-trip energy efficiency to 74%, while retaining the same level of current efficiency (99.7%) and capacity retention per cycle (99.95%) (Supplementary Fig. 9b).

Theoretical Modeling and Screening

One useful feature of organic electrolyte materials is the ability to optimize their properties through chemical modification, a process that can be accelerated by virtual testing with computational methods.[8,20] We assayed the chemical landscape around the

alloxazine backbone by computing the properties of derivatives bearing one to four copies of each of seven functional groups. Selected examples of alloxazine derivatives subjected to the theoretical modeling are shown in Table 3 (a complete table of the rest of the studied alloxazine derivatives can be found in supplementary table 1).

Figure 3 shows the variation in predicted standard reduction potential (E^0) within the alloxazine class. The additive effect of electron donating and electron withdrawing groups is observed as they lower and raise the reduction potential, respectively, across a range of 400 mV. Hydroxyl, methyl and methoxy substituents afford the largest increases in cell potential. We prepared 7/8-hydroxyalloxazine and 7,8-dimethylalloxazine via the aforementioned *o*-phenylenediamine-alloxan coupling chemistry (Table 2, Supplementary Fig. 10 and 11). CV of these two compounds showed values below −0.73 V (~110 mV lower than ACA), potentially raising the battery voltage by another 10% (Fig 3c and d).

In addition to tuning its reduction potential, modification of alloxazine with appropriate functional groups could also improve its chemical stability. Alloxazines undergo ring-opening reaction in aqueous solvent via addition of water to the amidic carbonyls followed by continuing hydrolysis to redox-inactive species (Supplementary Fig. 12).[21] Increases in pH catalyze the hydrolysis process, as observed in the FMN stability study and informed by literature.[22,23] Nevertheless, the low pK_a values at the amide nitrogen (8.4 and 11.4 for lumichrome[24]) result in the accumulation of two negative charges in the imidic conjugate system at high pH values; this process ultimately hinders the hydrolysis reaction by lowering the electrophilicity of the carbonyl groups.[25] Since the redox center and the center of electrophilic reactivity are separate in alloxazines,

184 design strategies are available to decrease chemical reactivity, such as tuning the
185 electrophilicity of alloxazines via different functional groups. We evaluated all the
186 screened alloxazines based on their predicted equilibrium constant, K_{hyd}, for the
187 reversible hydration of the carbonyl groups (Fig. 3b), with lower value of K_{hyd}
188 corresponding to less electrophilic carbonyls. We found that the same electron-donating
189 groups that contribute toward the desired reduction potential values also have a protecting
190 effect against hydrolysis, as is the case with amides in general (i.e. hydrolysis rate of
191 amides in basic medium has a linear dependence in K_{hyd}).[26] For instance, hydroxyl
192 derivatives lower K_{hyd} by as much as two orders of magnitude, thereby shifting the
193 equilibrium toward the redox-active "de-hydrated" form.

194 **Conclusions**

195 By drawing inspiration from vitamin B_2, we introduced a novel family of organic
196 molecules for RFB applications. The alloxazine redox-center exhibits sufficiently high
197 electrochemical and chemical stability, and sufficiently low reduction potential, to be
198 exploited as a negative electrolyte material in an alkaline RFB. Synthesis of a
199 functionalized alloxazine redox-active center was carried out via a very simple coupling
200 chemistry utilizing only *o*-phenylenediamine derivatives, alloxan, acetic acid and boric
201 acid, without employing high temperature or pressure. We paired alloxazine 7/8-
202 carboxylic acid with ferri/ferrocyanide to demonstrate a high-performance alloxazine-
203 powered RFB. The current efficiency exceeded 99.7% while its capacity retention over
204 400 charge-discharge cycles was shown to be ~95% cumulatively, or 99.98% per cycle.
205 With a better understanding of the alloxazine system enabled by theoretical modeling, we
206 have designed and characterized another two alloxazine-derived molecules promising

almost 10% further increase in battery voltage. The introduction of aza-aromatic redox-active species opens up a new direction in designing organic electrolyte and delivers a promising pathway to accelerate development of aqueous organic RFBs.

Methods

Chemical synthesis and characterization 3,4-diaminophenol was purchased from Aurum Pharmatech and used as received. All other chemicals were purchased from Sigma Aldrich and used as receieved. Alloxazines were prepared following previously reported methods.[14–16] In general, *o*-phenylenediamine (5 mmol) was added to 45 mL acetic acid followed by alloxan (5.5 mmol) and boric acid (5.5 mmol). The reaction mixture was stirred at room temperature and atmospheric pressure under nitrogen. The reaction times for various alloxazine derivatives are summarized in Table 2. After reaction, the product was collected by vacuum filtration, washed with acetic acid, water, and diethyl ether, and air dried overnight. The products were analyzed by ^{1}H NMR and used for chemical and electrochemical measurement without further purification. ^{1}H NMR spectra were recorded using Varian INOVA 500 (500 MHz) NMR spectrometers at 23 °C. Proton chemical shifts are expressed in parts per million (ppm, δ scale) and are referenced to residual protium in the NMR solvent (D_2O, δ 4.80 ppm and $(CD_3)_2SO$, δ 2.50 ppm). The isomeric ratio between major and minor product during the preparation of ACA and 7/8-hydroxyalloxazine was estimated based on their peak integration ratio (highlighted in Supplementary Fig. 2 and 10).

Stability test by ^{1}H NMR In a nitrogen-filled glove bag, a sample of ACA (0.5 M) was dissolved in a solution of 40% wt. KOD in D_2O (used as received from Sigma-Aldrich) which was then adjusted to pH 14 with the appropriate amount of D_2O. The sample was sealed inside a J. Young tube and analyzed by ^{1}H NMR. Analyses of the same sample were performed after 14, 21, 28, and 42 days. Between analyses, the J. Young tube was returned to the glove bag where it was kept in the dark. The proportion of ACA that had decomposed was determined by integrating the peaks at 6.48 ppm and comparing it to the peaks at 6.60 ppm and 6.86 ppm, which come from the starting material. From this data, the rate constant of ACA decomposition was calculated assuming first-order kinetics (Supplementary Fig. 4).

Solubility measurement by UV-Vis spectroscopy Saturated solution of ACA was prepared by addition of ACA to a pH 14 solution until precipitate formed. KOH was added if necessary to maintain the solution pH. Aliquots of the supernatant were diluted with a pH 14 KOH solution and its absorbance measured using UV-Vis spectrophotometry (Ocean Optics FLAME-S-UV-VIS; cuvettes are made out of polystyrene with a

path length of 1 cm). Readings were interpolated based on a standard calibration curve prepared by measuring the absorbance of known concentrations of ACA (Supplementary Fig. 13).

Electrochemical analysis Three-electrode cyclic voltammetry tests (CV) were performed using a glassy carbon working electrode, a Ag/AgCl reference electrode (pre-soaked in 3 M NaCl solution) and a platinum counter electrode. For the full cell measurements, cell hardware from Fuel Cell Tech. (Albuquerque, NM) was used to assemble a zero-gap flow cell configuration, similar to previous reports.[27] POCO graphite flow plates with serpentine flow fields were used for both sides. A 5 cm^2 geometric surface area electrode comprised a stack of two or three sheets of Sigracet SGL 10AA porous carbon paper, pretreated by baking in air at 400 °C for 24 h. A sheet of Nafion 212 membrane, pretreated in DI water overnight, served as the ion-selective membrane. The rest of the space between the plates was gasketed by either Kalrez or Teflon sheets. The electrolytes were fed into the cell through PFA tubing, at a rate of 60 mL/min controlled by Cole-Parmer Masterflex L/S peristaltic pumps. All electrochemical tests were performed using a Gamry Reference 3000 potentiostat.

Rotating disk electrode (RDE) measurement RDE experiments were conducted using a BASi RDE (RDE-2) instrument equipped with a glassy carbon working electrode, a Ag/AgCl reference electrode (pre-soaked in 3 M NaCl solution) and a platinum counter electrode. The electrode was rotated at a specific speed while the voltage was linearly swept from −0.70 V to −1.20 V versus Ag/AgCl. The reduction rate constant of ACA was calculated from the ~~Bulter-Volmer~~Tafel equation using the following parameters: n = 2; Faraday's constant F = 96,485 C mol^{-1}; electrode area A = 0.0707 cm^2, ACA concentration $C = 2 \times 10^{-6}$ mol cm^{-3}; kinematic viscosity $\nu = 0.01$ cm^2 s^{-1} (Supplementary Fig. 3**).** The experiment was performed three times.

Electrolyte preparation For SOC, polarization and 400-cycle charge-discharge studies, the positive electrolyte was prepared by dissolving ferrocyanide (1.9 g, 4.5 mmol) and ferricyanide (0.15 g, 0.46 mmol) in 1 M KOH solution (11.25 mL) to afford 0.4 molar electron concentration and 2.7 molar K^+ ion solution (11 Ah/L charge density). The negative electrolyte was prepared by dissolving ACA (0.39 g, 1.5 mmol) in 2.5 M KOH solution (adjusted to final volume of 3 mL) to afford 1 molar electron concentration and 2 molar K^+ ion solution (27 Ah/L charge density). For high concentration ACA cycling experiment, the

positive electrolyte was prepared by dissolving ferrocyanide (3.8 g, 9 mmol) and ferricyanide (0.3 g, 0.91 mmol) in 1 M KOH solution (22.5 mL) to afford 0.4 molar electron concentration and 2.7 molar K^+ ion solution (11 Ah/L charge density). The negative electrolyte was prepared by dissolving ACA (0.78 g, 3 mmol) in 4 M KOH solution (adjusted to final volume of 3 mL) to afford 2 molar electron concentration and 4 molar K^+ ion solution (54 Ah/L charge density).

Computational studies

Libraries considered. We have analyzed all the possible substitutions for each functional group on all the possible sites of the alloxazine core. The functional groups assessed are carboxylic acid, fluoro, hydroxyl, methoxy, methyl, phosphonic acid and sulfonic acid. Substitution on the alloxazine amide nitrogens were not considered as they destabilize alloxazines under alkaline condition. A total of 105 backbones were analyzed.

~~*General methods.*~~ Initial conformations were generated that used a random-distance matrix approach at the mmff94 level of theory. Geometries were further refined using DFT and single-point calculations were performed using larger basis sets and solvent corrections. The following methods were tested for obtaining equilibrium geometries and total energies: PM7, PM7 + implicit COSMO solvation, PBE/6-31G*, B3LYP/6-31G*. In addition, single point calculations were performed at both B3LYP/6-311+G(d,p) and B3LYP/6-311+G(d,p) combined with CPCM implicit solvation. Their relative performance is compared in the supplementary information file. For both target properties we obtained the smallest error using B3LYP/6-311+G(d,p) CPCM.

~~*Reduction potential.*~~ Reduction potentials were predicted from the energy difference between the reduced and oxidized forms of alloxazines, assuming a two-electron two-proton process. Prior to conducting predictions, we assessed the performance of various quantum chemical methods to calculate the two-proton two-electron redox potential of alloxazine and isoalloxazine rings at pH = 7.4 using a calibration scheme analogous to the one reported for quinones. The calibration dataset was composed of 23 experimentally-reported molecules, with $E^0_{pH=7}$ ranging between −380 meV and −80 meV versus RHE.[28] Our results suggest that quick semiempirical methods and gas-phase DFT calculations afford results with mean errors

around 20 meV. DFT calculations in implicit solvent with a larger basis set reduce the average error to under 10 meV. The performance of various methods is reported in Supplementary Table 2.

We then corrected E^0 values to pH = 14.0. Pourbaix diagrams were estimated combining experimental and predicted pK_a values (pK_a^{ox} = 8.3, 11.4; pK_a^{red} = 6.7, 10.0). The shift from pH = 7.4 to pH = 14.0 for alloxazines is thus estimated at −320 meV. To calculate

hHydration equilibrium, ~~W~~we used an experimental dataset from the literature including aldehydes, ketones, esters and amides and mapped theoretical reaction energies at 0 K to experimentally-determined hydration equilibrium constants in water.[29]. The calibration dataset was composed of 41 experimentally-reported molecules, with logK_{hyd} ranging between −15 and 5. DFT calculations in implicit solvent result in mean errors close to 1 log unit. The performance of various methods is reported in Supplementary Table 2.

Formatted: Font: Not Italic

299 **References**

300 1. Dunn, B., Kamath, H. & Tarascon, J.-M. Electrical Energy Storage for the Grid: A
301 Battery of Choices. *Science* **334,** 928–935 (2011).
302 2. Nguyen, T. & Savinell, R. F. Flow Batteries. *Electrochem. Soc. Interface* **19,** 54–56
303 (2010).
304 3. Yang, Z. *et al.* Electrochemical Energy Storage for Green Grid. *Chem. Rev.* **111,**
305 3577–3613 (2011).
306 4. Biello, D. Solar Wars. *Sci. Am.* **311,** 66–71 (2014).
307 5. Skyllas-Kazacos, M., Chakrabarti, M. H., Hajimolana, S. A., Mjalli, F. S. & Saleem,
308 M. Progress in Flow Battery Research and Development. *J. Electrochem. Soc.* **158,**
309 R55–R79 (2011).
310 6. Weber, A. Z. *et al.* Redox flow batteries: a review. *Journal of Applied*
311 *Electrochemistry* 41, 1137-1164 (2011).
312 7. Perry, M. L. & Weber, A. Z. Advanced Redox-Flow Batteries: A Perspective. *J.*
313 *Electrochem. Soc.* **163,** A5064–A5067 (2016).
314 8. Huskinson, B. *et al.* A metal-free organic-inorganic aqueous flow battery. *Nature* **505,**
315 195–198 (2014).
316 9. Huskinson, B., Marshak, M. P., Gerhardt, M. R. & Aziz, M. J. Cycling of a Quinone-
317 Bromide Flow Battery for Large-Scale Electrochemical Energy Storage. *ECS Trans.*
318 **61,** 27–30 (2014).
319 10. Lin, K. *et al.* Alkaline quinone flow battery. *Science* **349,** 1529–1532 (2015).
320 11. Janoschka, T. *et al.* An aqueous, polymer-based redox-flow battery using non-
321 corrosive, safe, and low-cost materials. *Nature* **527,** 78–81 (2015).

12. Schubert, U. S. *et al.* Polymer/Zinc Hybrid-Flow Battery Using Block Copolymer Micelles featuring a TEMPO Corona as Catholyte. *Polym Chem* **28**, 2238-2243 (2016).
13. Liu, T., Wei, X., Nie, Z., Sprenkle, V. & Wang, W. A Total Organic Aqueous Redox Flow Battery Employing a Low Cost and Sustainable Methyl Viologen Anolyte and 4-HO-TEMPO Catholyte. *Adv. Energy Mater.* **6**, 1501449 (2015).
14. Chen, S., Hossain, M. S. & Foss, F. W. Organocatalytic Dakin Oxidation by Nucleophilic Flavin Catalysts. *Org. Lett.* **14,** 2806–2809 (2012).
15. Gonzalo, G. de, Smit, C., Jin, J., Minnaard, A. J. & Fraaije, M. W. Turning a riboflavin-binding protein into a self-sufficient monooxygenase by cofactor redesign. *Chem. Commun.* **47,** 11050–11052 (2011).
16. Lindén, A. A., Johansson, M., Hermanns, N. & Bäckvall, J.-E. Efficient and Selective Sulfoxidation by Hydrogen Peroxide, Using a Recyclable Flavin−[BMIm]PF6 Catalytic System. *J. Org. Chem.* **71,** 3849–3853 (2006).
17. Hasford, J. J. & Rizzo, C. J. Linear Free Energy Substituent Effect on Flavin Redox Chemistry. *J. Am. Chem. Soc.* **120,** 2251–2255 (1998).
18. Müller, F. in *Radicals in Biochemistry* 71–107 (Springer, 1983).
19. Hong, J. *et al.* Biologically inspired pteridine redox centres for rechargeable batteries. *Nat. Commun.* **5,** (2014).
20. Er, S., Suh, C., Marshak, M. P. & Aspuru-Guzik, A. Computational design of molecules for an all-quinone redox flow battery. *Chem Sci* **6,** 885–893 (2015).
21. Koziol, J. & Metzler, D. E. Formation and Possible Structure of Covalent Hydrates of Alloxazines. *Z. Für Naturforschung B* **27,** 1027–1029 (2014).

22. Surrey, A. R. & Nachod, F. C. Alkaline Hydrolysis of Riboflavin. *J. Am. Chem. Soc.* **73,** 2336–2338 (1951).

23. Ahmad, I., Rapson, H. D. C., Heelis, P. F. & Phillips, G. O. Alkaline hydrolysis of 7,8-dimethyl-10-(formylmethyl)isoalloxazine. A kinetic study. *J. Org. Chem.* **45,** 731–733 (1980).

24. Prukała, D. *et al.* Acid–Base Equilibriums of Lumichrome and its 1-Methyl, 3-Methyl, and 1,3-Dimethyl Derivatives. *J. Phys. Chem. A* **116,** 7474–7490 (2012).

25. Koziol, J., Tyrakowska, B. & Müller, F. The structure of covalent hydrates of alloxazines. A reinvestigation. *Helv. Chim. Acta* **64,** 1812–1817 (1981).

26. O'Connor, C. Acidic and basic amide hydrolysis. *Q. Rev. Chem. Soc.* **24,** 553–564 (1970).

27. Liu, Q. H. *et al.* High Performance Vanadium Redox Flow Batteries with Optimized Electrode Configuration and Membrane Selection. *J. Electrochem. Soc.* **159,** A1246–A1252 (2012).

28. Li, X.-L. & Fu, Y. Theoretical study of reduction potentials of substituted flavins. *J. Mol. Struct. THEOCHEM* **856,** 112–118 (2008).

29. Gómez-Bombarelli, R., González-Pérez, M., Pérez-Prior, M. T., Calle, E. & Casado, J. Computational Calculation of Equilibrium Constants: Addition to Carbonyl Compounds. *J. Phys. Chem. A* **113,** 11423–11428 (2009).

Acknowledgements

This work was funded by the U.S. DOE ARPA-E award # DE-AR0000348. and NSF # NSF-CBET-1509041. We thank Chenxi Qian for designing the Figure 1d scheme.

Author ~~e~~Contributions

K.L., R.G.G. and M.J.A. formulated the project. K.L., and L.T. synthesized the compounds. K.L., E.S.B. and L.T. collected and analyzed the NMR data. K.L., Q.C., E.S.B. and A.V. collected and analyzed the electrochemical data. K.L. and A.V. measured solubility. R.G.B. and A.A.-G. performed theoretical analysis. K.L., R.G.G. and M.J.A. wrote the paper, and all authors contributed to revising the paper.

Additional Information

Supplementary information is available online. Reprints and permissions information is available online at www.nature.com/reprints. Correspondence and requests for materials should be addressed ~~Supplementary information is available online. Correspondence and requests for materials should be addressed~~ to R.G.G and M.J.A.

Formatted: Font: Not Italic

Formatted: Font: Not Italic

Formatted: Font: Not Italic

Competing interests

The authors declare no competing financial interests.

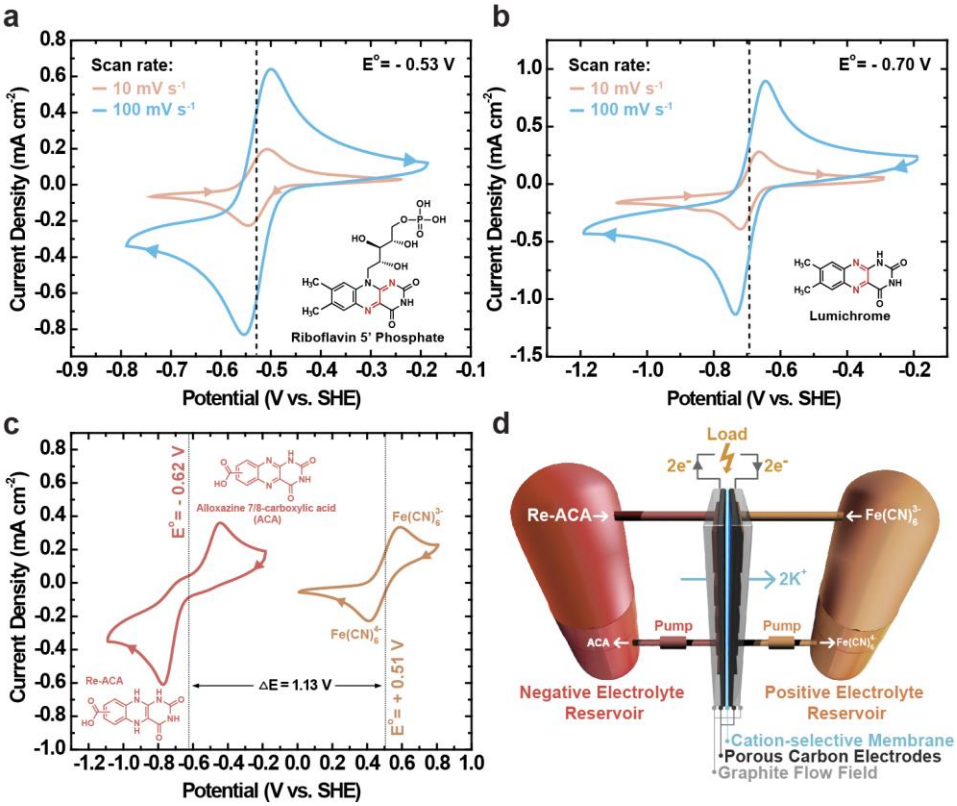

Figure 1 | Cyclic Voltammogram and Cell Schematic. a and **b**, Molecular structures and cyclic voltammogram of 2 mM riboflavin 5' phosphate (FMN) and lumichrome, respectively, scanned at 10 mV/s and 100 mV/s on glassy carbon electrode. **c**, Cyclic voltammogram of 2 mM alloxazine 7/8-carboxylic acid (ACA) (red curve) and ferrocyanide (gold curve) scanned at 100 mV/s on glassy carbon electrode; arrows indicate scan direction. **d**, Schematic of cell in discharge mode. Grey arrow indicate flow direction of electrons and white arrows indicate electrolyte solution flow. Blue arrow indicates migration of cations across the membrane. Essential components of electrochemical cells are labeled with color-coded lines and text.

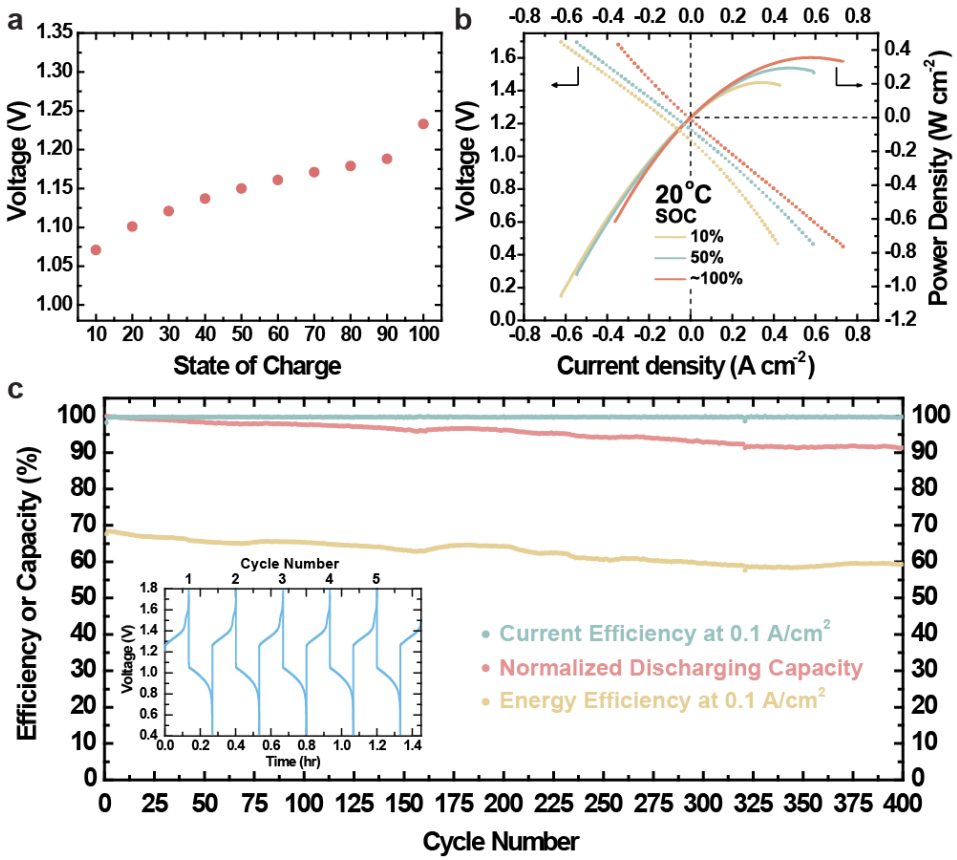

Figure 2 | Cell Performance (a) Cell open-circuit voltage (OC~~P~~V) vs. state-of-charge (SOC). All potentials were taken when the cell voltage stabilized to within ± 1 mV. 100% SOC was reached by a potentiostatic hold at 1.5 V until the current decreased to below 5 mA/cm^2. **(b)** Cell voltage & power density vs. current density at 20 ^{o}C, at 10%, 50%, and ~100% SOC. Electrolyte composition: 0.5 M ACA and 0.4 M ferrocyanide + 40 mM ferricyanide were used in negative electrolyte and positive electrolyte, respectively. **(c)** Capacity retention, current efficiency and energy efficiency values over 400 cycles at 0.1 A/cm^2. The normalized discharging capacity is evaluated based on the capacity of the first discharge cycle. (Inset: Representative voltage vs. time curves during 400 charge-discharge cycles at 0.1 A/cm^2, recorded between the 1st and 5th cycles.)

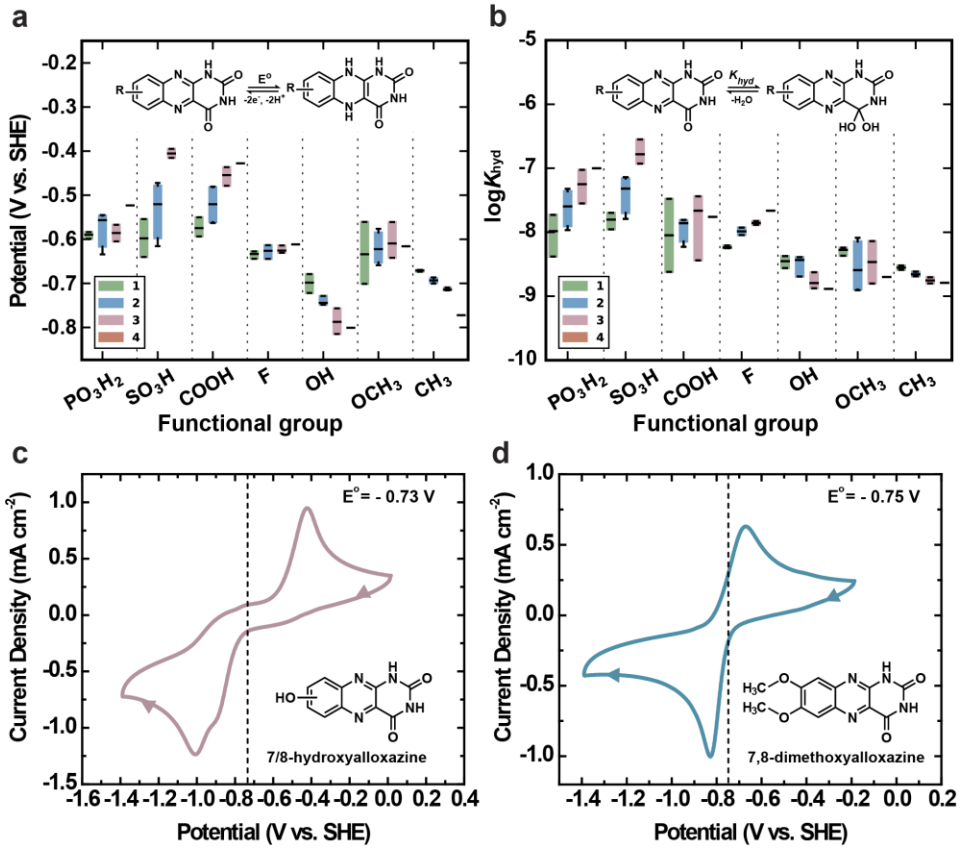

Figure 3 | Theoretical Calculation and Cyclic Voltammetry of alloxazines. (a) Predicted reduction potential at the B3LYP 6-311+G** CPCM level of theory for substituted alloxazines at pH=14.0 vs. RHE as a function of number and type of substituent. ~~Bars range from first to third quartile, whiskers extend across the range, and horizontal lines mark the mean.~~ **(b)** Predicted logK_{hyd} at the B3LYP 6-311+G** CPCM level of theory for substituted alloxazines as a function of number and type of substituent. The bars represent the statistical distribution of predictions of all the possible substituted molecules with the given number of substituted sites. The bottom and top of the bar are the first and third quartiles, and the band inside the box is the median. The lines extending vertically from the boxes indicate the maximum and minimum of the range. **(c)** and **(d)** Molecular structures and cyclic voltammogram of 1 mM 7/8-hydroxyalloxazine and 7,8-dimethoxyalloxazine, respectively, scanned at 100 mV/s on glassy carbon electrode.

Table 1 | High Performance Organic-based Aqueous Redox Flow Batteries. [a]This table focuses primarily on comparing molecular structures of redox-active organic molecules and evaluating their electrochemical stability based on capacity retention.

Positive Electrolyte	Negative Electrolyte	No. of Cycles (Condition)	Capacity Retention per Cycle (%)[a]	Energy Density (Wh/L)	Voltage (V)	Year of Publication	Me (limita
bromine/ hydrobromic acid	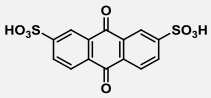 anthraquinone-2,7-disulfonic acid	10	99	16	0.86	2014[8]	Low co hig perfor (tox brom
		750	99.84	16		2014[9]	
ferrocyanide	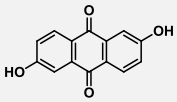 2,6-dihydroxy-anthraquinone	100	99.1	6.8	1.2	2015[10]	Non-toxic and less corrosive electrolyte (reduced ion conductivity w.r.t. proton)
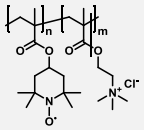 TEMPO polymer	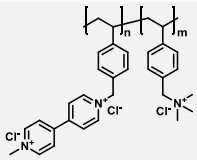 viologen polymer	100	~ 99.75[b,e]	10	1.15	2015[11]	Cheap dialysis membrane (high electrolyte viscosity)
		10,000 (non-flow cell)	> 99.99				
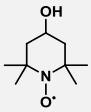 4-hydroxy-TEMPO	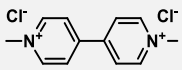 methyl viologen	100 (low conc.)	> 99.99	8.4	1.25	2015[13]	Low cost all-organic electrolyte (low current density)
		100 (high conc.)	99.89				

[a] ~~This table focuses primarily on comparing molecular structures of redox-active organic molecules; capacity retention was used as a method to evaluate their electrochemical stability.~~

[b]Capacity retention per cycle was derived from total capacity retention divided by total number of charge-discharge cycles.

[b,e] The capacity retention value was estimated based on the capacity retention vs. cycle number graph in figure 4 from reference 11.

Formatted: Don't add space between paragraphs of the same style, Line spacing: single

Formatted: Font: Bold

Formatted: Font: 12 pt

Formatted: Font: 12 pt

Formatted: Font: 12 pt

Formatted: Font: 12 pt

Formatted: Font: 10 pt, Not Superscript/ Subscript

Formatted: Superscript

Table 2 | Reaction Scheme and Summary of Alloxazine Synthesis from Literature.

Alloxazines with different functional groups (-R) can be prepared by coupling *o*-phenylenediamine derivatives with alloxane in the presence of acetic acid and boric acid.

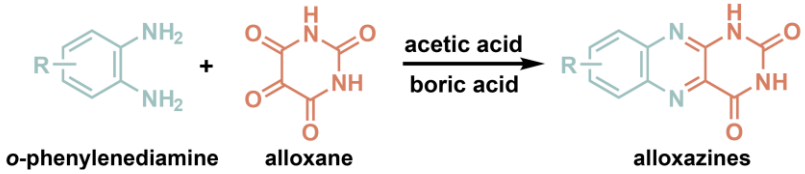

o-phenylenediamine alloxane alloxazines

o-phenylenediamine	alloxazines	Reaction Time (h)	Yield (%)	Reference
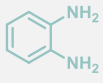	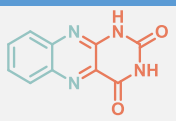 alloxazine	2	**87**	Chen *et al.*[14]
			95	Gonzalo *et al.*[15]
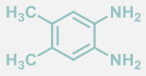	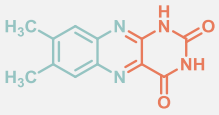 lumichrome	2	**95**	Chen *et al.*[14]
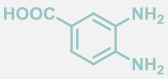	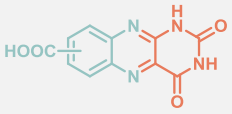 alloxazine 7/8-carboxylic acid (ACA)	3	**100**	Linden *et al.*[16]
			95	*This work*
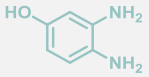	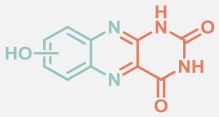 7/8-hydroxyalloxazine	3	**86**	*This work*
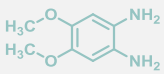	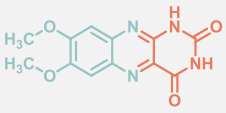 7,8-dimethoxyalloxazine	2	**89**	Chen *et al.*[14]
			94	*This work*

Formatted: Line spacing: single

Formatted: Font: Bold

Formatted: Font: Italic

Formatted: Font: (Default) Times New Roman, 12 pt

Table 3 |. Theoretical Calculation and Substitution Ppatterns of Alloxazines. and **p**Predicted standard reduction potential (E^o) and logarithmic hydration equilibrium constant ($\log K_{hyd}$) for alloxazines with hydroxyl functional group(s).

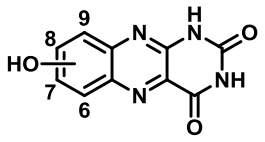

hydroxylated alloxazines

No.	Position (-OH)				B3LYP 6-311+G** CPCM	
	6	7	8	9	E^o (V)	$\log K_{hyd}$
1 Substituent						
1	H	H	H	-OH	−0.69	−8.4
2	H	H	-OH	H	−0.72	−8.7
3	H	-OH	H	H	−0.68	−8.5
4	-OH	H	H	H	−0.77	−8.3
2 Substituents						
5	-OH	-OH	H	H	−0.75	−8.4
6	-OH	H	-OH	H	−0.71	−8.6
7	-OH	H	H	-OH	−0.77	−8.2
8	H	-OH	-OH	H	−0.76	−9.3
9	H	-OH	H	-OH	−0.68	−8.4
10	H	H	-OH	-OH	−0.73	−8.7
3 Substituents						
11	-OH	-OH	-OH	H	−0.81	−8.9
12	-OH	-OH	H	-OH	−0.74	−8.3
13	-OH	H	-OH	-OH	−0.82	−8.7
14	H	-OH	-OH	-OH	−0.74	−8.9
4 Substituents						
15	-OH	-OH	-OH	-OH	−0.80	−8.9

Formatted: Font: Bold

Formatted: Font: Bold

Formatted: Font: Bold

Formatted: Font: Bold

Formatted: Font: Bold